Effect of Tropical Cyclone Intensity on the Relationship between Hydrometeor Distribution and Rapid Intensification by GPM GMI

Yuankang Leng[1], Rui Liu[1], Peijun Zhu[1], and Honglei Zhang[2]

[1]School of Earth Sciences, Zhejiang University, Hangzhou, China

[2] Zhejiang Institute of Meteorological Sciences, Hangzhou, China

Corresponding author: Peijun and Zhu (zhupj@zju.edu.cn)

Key Points:

- Hydrometeor contents increase in the whole area of a weak TC but mainly in the inner-core of a strong TC during rapid intensification (RI).
- Hydrometeor contents are higher in RI than in slow intensification, and the maxima locate related to TC intensity and intensification rate.
- The cloud water content in the inner-core area have the largest correlation with the TC intensification rate, especially in a weak TC.

Abstract

This study analyzes hydrometeor evolution during rapid intensification (RI) and tropical cyclone (TC) intensity dependence using satellite data. Previous studies have suggested that ice cloud water or non-convective precipitation can serve as predictors of RI from different perspectives. However, few studies have focused on the impact of TC intensity or comprehensive comparisons to identify better indicators. During RI, the hydrometeor contents in weak TCs (WTCs) increase over the entire region, whereas they increase mainly in the inner-core region and decrease in advance in the outer-core region for strong TCs (STCs). Hydrometeor contents are higher in RI than in slow intensification, and their maximum locations are related to TC intensity and intensification rate. Cloud water content (CWC) in the inner-core region has the largest correlation with the intensification rate, especially in WTCs. Therefore, the CWC can serve as a predictor of RI and can be applied to all TC intensities.

Plain Language Summary

Stronger tropical cyclones (TCs), which often undergo rapid intensification (RI), cause significant damage. However, accurately predicting its intensity is difficult. A close relationship exists between TC intensity changes and cloud content. Previous studies have shown a connection between the ice water content, precipitation, and RI of TCs. However, few studies have comprehensively compared the hydrometeors and precipitation associated with RI and the impact of TC intensity. During the RI, various cloud contents increase in the entire area of a weak TC, while they increase mainly in the inner-core area and decrease in advance in the outer-core area of a strong TC. The cloud contents are higher in RI than in slow intensification, and their maximum locations are related to the TC intensity and intensification rate. Among the cloud content and precipitation types, the water cloud content in the TC inner-core area is the

best indicator of the intensification rate, applicable to all TC intensities, especially for weak TCs. Understanding the relationship between clouds and TC intensification facilitates prediction of TC intensity and reduces the impact of disasters.

1 Introduction

Tropical cyclones (TCs) are one of the most destructive weather systems worldwide. Significant progress has been achieved in predicting TC intensity; however, predicting the rapid intensification (RI) of TC remains challenging (Kaplan et al., 2010; Courtney et al., 2019; DeMaria et al., 2021). This is primarily due to the limited understanding of the physical processes responsible for TC intensity changes, especially for RI (Elsberry et al., 2007; Kaplan et al., 2010; Emanuel, 2018). Over the past few decades, the frequency and magnitude of RI have gradually increased, and the location of RI has notably become considerably closer to the coast (Zhao et al., 2018; Song et al., 2020; Klotzbach et al., 2022; Liu & Chan, 2022; Li et al., 2023). Therefore, understanding the RI process from various perspectives is imperative to improve the accuracy of RI forecasting and reduce disaster losses.

Previous theoretical studies have demonstrated that the evolution of TC intensity is closely related to latent heat release and that the maximum intensifying efficiency occurs when latent heating is within the radius of the maximum wind (RMW) (Shapiro & Willoughby, 1982; Schubert & Hack, 1982; Vigh & Schubert, 2009; Rogers et al., 2013). Simulation analysis has also shown a strong correlation between the total heating and total condensate water within the TC (Nolan et al., 2019). Recent studies have suggested that convective bursts (CBs) can serve as precursors to the RI, especially the frequency of CBs in the core region, which increases before the RI (Rogers et al., 2013; Wang & Wang, 2014; Miller et al., 2015). Tang et al. (2019) found that deep convection and the associated latent heat increased substantially, shifting inward before the onset of RI. Further studies have revealed that ice-phase microphysical processes in the upper troposphere play an important role in RI (Zhao et al., 2020). Though most of simulation studies have focused on the core area where the cloud microphysical processes are sensitive to TCs structures and intensities (Lord et al., 1984; Sawada & Iwasaki, 2007; Zhu & Zhang, 2006; Pattnaik & Krishnamurti, 2007), diabatic heating resulting from cloud microphysical processes in outer spiral rainbands can also affect TC intensity (Wang, 2009).

Although it is challenging to directly measure the amount of latent heat that can be converted into potential and kinetic energies within a TC using observational data, hydrometeors are a feasible proxy (Adler & Rodgers, 1977; Rodgers et al., 1994; Rodgers & Pierce, 1995). Microwave radiation observations have been used for decades to identify TC intensification signals. Ice-scattering signals in microwave bands are highly correlated with future TC intensity (Cecil & Zipser, 1999; Kieper & Jiang, 2012; Harnos & Nesbitt, 2016). Harnos and Nesbitt (2016) found that the 85-GHz channels bright temperatures of intensifying TCs are lower than that of weakening TCs, implying a stronger signal of ice-phase particle scattering. More precipitation and colder clouds have been observed with TC intensification (Ruan and Wu, 2018). Therefore, the ice-phase condensate content can serve as an indicator of TC intensification (Wu & Soden, 2017; Su et al., 2020; Zhang et al., 2019). Furthermore, Wu et al. (2020) revealed that the ice water content in the upper troposphere is highly correlated with the TC intensification rate, and Liu et al. (2022) suggested that the radial distribution of the deep convective cloud percentage and temperature could be used to identify the impending RI.

However, some studies have considered that deep convective activities are more likely to be a response rather than a precursor to RI, as they increase significantly after the onset of RI (Jiang & Ramirez, 2013; Zagrodnik & Jiang, 2014; Tao & Jiang, 2015; Tao et al., 2017; Fisher et al., 2018). Statistical analysis of the precipitation characteristics of intensifying TCs by Jiang and Ramirez (2013) indicated that the maximum convective precipitation intensity in the inner-core region is not necessarily more intense for an RI episode than for a non-RI episode. Tao and Jiang (2015) showed that increased and widespread shallow precipitation has occurred in the TC core area before RI and which contributes to higher total volumetric rainfall and latent heat than non-RI, suggesting that RI is probably triggered by the increase of shallow-moderate precipitation. Therefore, stratiform precipitation may be a dominant factor in the RI (Zagrodnik & Jiang, 2014; Fisher et al., 2018; Tao et al., 2017). Due to the different study perspectives it is hard to know if IWC or non-convective precipitation is the better predictor, though they varies coinstantaneous during TC intensification.

Observational and modeling studies have indicated a relationship between TC intensification rate and intensity (Shapiro and Willoughby, 1982; Xu and Wang, 2015). Stronger TCs demonstrate higher inertial stability within the RMW region, resulting in increasing intensification efficiency and tangential wind tendencies in response to the latent heat in the eyewall (Schubert and Hack., 1982). Nolan et al. (2007) suggested that the intensification efficiency is positively related to the intensity of weak storms. Wu et al. (2020) found that TC experiencing an RI tends to have a higher initial intensity than more slowly intensifying TC. The relationship between TC intensity and the intensification rate is complex and nonlinear (Xu & Wang, 2015; Wang et al., 2021). Therefore, questions arise regarding the main differences in cloud microphysical characteristics between RI and slow-intensification (SI) processes in the context of different TC intensities. Furthermore, which is the key indicator of the RI process, hydrometeor or precipitation, and are they influenced by TC intensity? The objective of this study is to answer these questions using Global Precipitation Measurement (GPM) satellite observations, which have been widely used in cloud and precipitation studies. The remainder of this paper is organized as follows: The data and methods are described in Section 2, the main results are presented in Section 3, and the conclusions are discussed in Section 4.

2 Data and Methods

In this study, we utilite GPM observations of the rain water content (RWC), ice water content (IWC, solid), cloud water content (CWC, liquid), and the column mass-integrated contents including rainwater path (RWP), ice water path (IWP), and cloud water path (CWP) (Hou et al., 2014, Randel et al., 2020). Surface and convective precipitation rates are also used. These data are retrieved from the passive microwave data product (2AGRPOFGMI) on the GPM with a resolution of 13 × 13 km and an interval of approximately 90 min. Pixel-level surface precipitation rate and vertical hydrometeor content distribution files are generated using the Goddard Profiling Algorithm (GPROF, Randel et al., 2020).

The International Best Track Archive for Climate Stewardship (IBTrACS, Knapp et al., 2010) provides the TC location and maximum wind speed at 6-h intervals from March 2014 to December 2022 over the western North Pacific (WNP). Following the definition given by Kaplan and Demaria (2003), an RI case is defined as an increase of TC surface maximum wind speed of at least 30 kts within 24 h ($\Delta V_{RI} \geq 30$kt, $\Delta V = V_{24h} - V_{0h}$). For comparison, we also select slow intensification (SI) cases with an intensification rate of less than 30 kts per 24-h (30 kts $> \Delta V_{SI} > 0$ kt). The radius of maximum wind (RMW) data is provided by IBTrACS.

Owing to the time inconsistency between GPM observations and TC data, the former has a higher temporal resolution at a 90-min interval while the latter is at a 6-h interval. The TC data are first linearly interpolated to match the observation time of GPM satellite. Then, swath data within 500 km of the TC center are directly extracted. Owing to the satellite orbit and scanning method, the number of TCs that can be scanned by the GPM is far less than the total number of TCs. However, their frequency distributions based on TC intensity for RI and SI are almost the same, indicating that the episodes scanned by GPM are representative of the initial intensities of the intensification episodes (Fig. S1; the numbers of cases are shown in Table S1).

The initial intensity of the intensification episodes is predominantly distributed in the 30–90 kts (Table S1). Therefore, in this study, the RI and SI cases are categorized into two groups based on the initial intensity: $TC_{30\text{-}60kt}$ (the initial intensity in the range of 30–60 kts) and $TC_{60\text{-}90kt}$ (the initial intensity in the range of 60–90 kts) representing weak and strong TCs, respectively. All cases represented RI or SI with an initial intensity of 30–90 kts. In addition, we define the inner-core, outer-core, and outer regions of the TC with radii of 100, 100–300, and 300–500 km from the TC center, respectively. The radii of the inner-core and outer-core regions are similar to those defined by Weatherford and Gray (1988a). Weatherford and Gray (1988a and 1988b) found that the outer-core region wind strength is weakly related to the inner-core intensity unless the eye structures are considered, which are closely linked to the TC intensity.

3 Results

The time evolutions of the hydrometeor content within a 500 km radius of TC are analyzed for both the RI and SI cases. Because the evolution features of RWP, IWP, and CWP are similar, only CWP is presented in Fig. 1 as a representative example; those of RWP and IWP are shown in Fig. S2 for details. For all intensifying cases (black curves in Fig. 1a and 1e, Fig. S2), RWP, IWP, and CWP increase during the RI process but are essentially unchanged in SI; therefore, after 24-h the hydrometeor contents of RI are larger than those of SI, although they are opposite at the onset. This implies that the change in hydrometeor content is closely related to the change in TC intensity. The hydrometeor contents of the $TC_{60\text{-}90kt}$ cases are higher than those of the

$TC_{30\text{-}60kt}$ cases both in the RI and SI processes, although their increasing rates are relatively different (Fig. 1a and 1e). During RI, the $TC_{30\text{-}60kt}$ cases have higher changes in hydrometeor contents than those of the $TC_{60\text{-}90kt}$ cases, while the opposite is true in SI. There are two notable phenomena: the hydrometeor content changes in the 24-h period of the $TC_{60\text{-}90kt}$ cases in RI and SI are nearly the same, and the hydrometeor content changes of $TC_{30\text{-}60kt}$ during SI are nearly zero. This implies that the hydrometeor content changes vary significantly with TC intensity and intensification rate.

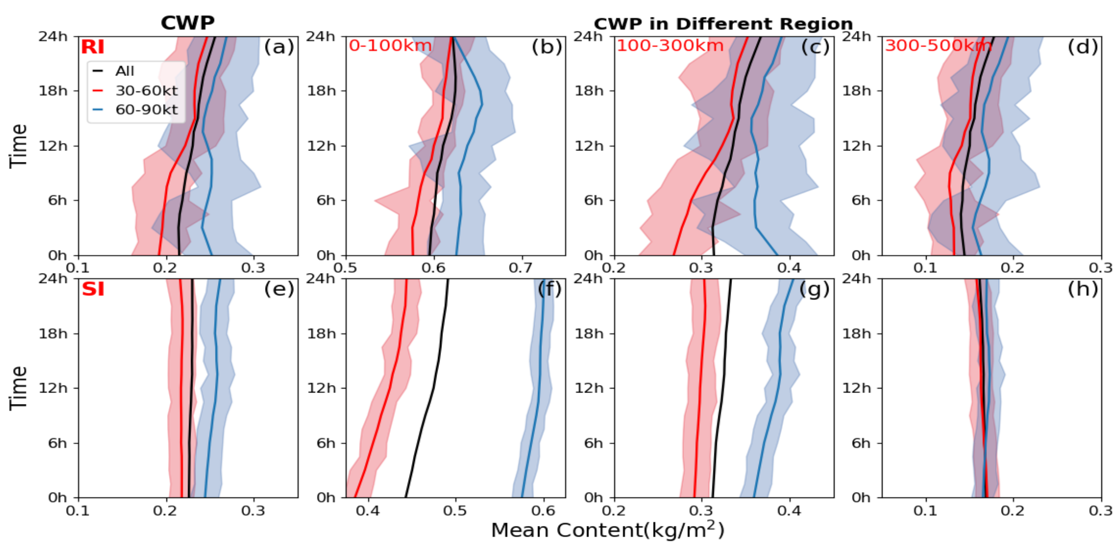

Fig. 1 Evolution of averaged CWP (kg/m^2) within the radius of 500 km in RI (a) and SI (e) for all intensifying cases. Black, red, and blue lines denote the average contents for all, $TC_{30\text{-}60kt}$, and $TC_{60\text{-}90kt}$ cases, respectively. (b-d) and (f-h) similar to (a, e) but over an area within radii of 100, 100–300, and 100–500 km, respectively. The shading represents 95% confidence intervals for average CWP.

Fig. 1b-1d and Fig. 1f-1h further show the CWP evolutions in the inner-core, outer-core and outer regions of the TC. A significant difference is observed in hydrometeor content among these regions (see Fig. S3 for the consecutive radial distributions). The CWP is predominantly largest in the core area of the TC, regardless of the RI or SI cases (Fig.1b and 1f), where strong updrafts appeared with dominant water vapor convergence in the lower troposphere. CWP in the $TC_{60\text{-}90kt}$ inner-core region increases slowly at first and starts to rapidly increase in 9 h after the onset of RI, reaching a maximum at approximately 16 h and then weakening (Fig. 1b). The evolution of CWP in the outer-core region for strong TCs is almost opposite, decreasing rapidly in the first 3 h, slowly decreasing, and then reaching a minimum approximately 1 h early than the time of maximum in the inner-core region (Fig. 1c). This shows the contraction feature of the CWP in the outer-core region of strong TCs first, followed by an increase in the CWP in the inner-core region. In $TC_{30\text{-}60kt}$, however, the CWP evolution for RI is significantly different, increasing in almost all regions for RI (Fig. 1b-1d). The different features of weak and strong TCs can be demonstrated through the lead-lag correlation analysis between these two regions (Table S2). $TC_{30\text{-}60kt}$ cases exhibit a significant positive correlation between CWPs in the inner-core and outer-core regions, while $TC_{60\text{-}90kt}$ show a significant negative correlation, especially when the evolution of the hydrometeor in the outer-core region led to 3 h. This might be the different models of hydrometeor content increase in the inner-core region for the weak and strong TCs associated with those in the outer-core region. In a recent study on the super-Typhoon Nanmadol (2022), it is found that there is a small amount of large particle region approximately 300 km from the eye in the post-period of RI (Wu et al., 2023). This implies that the outer-core region of strong TCs is a particular area of hydrometeor evolution during the RI. The CWP in the outer region is much smaller than that in the core regions, and is its change over a short time (Fig. 1d and 1h).

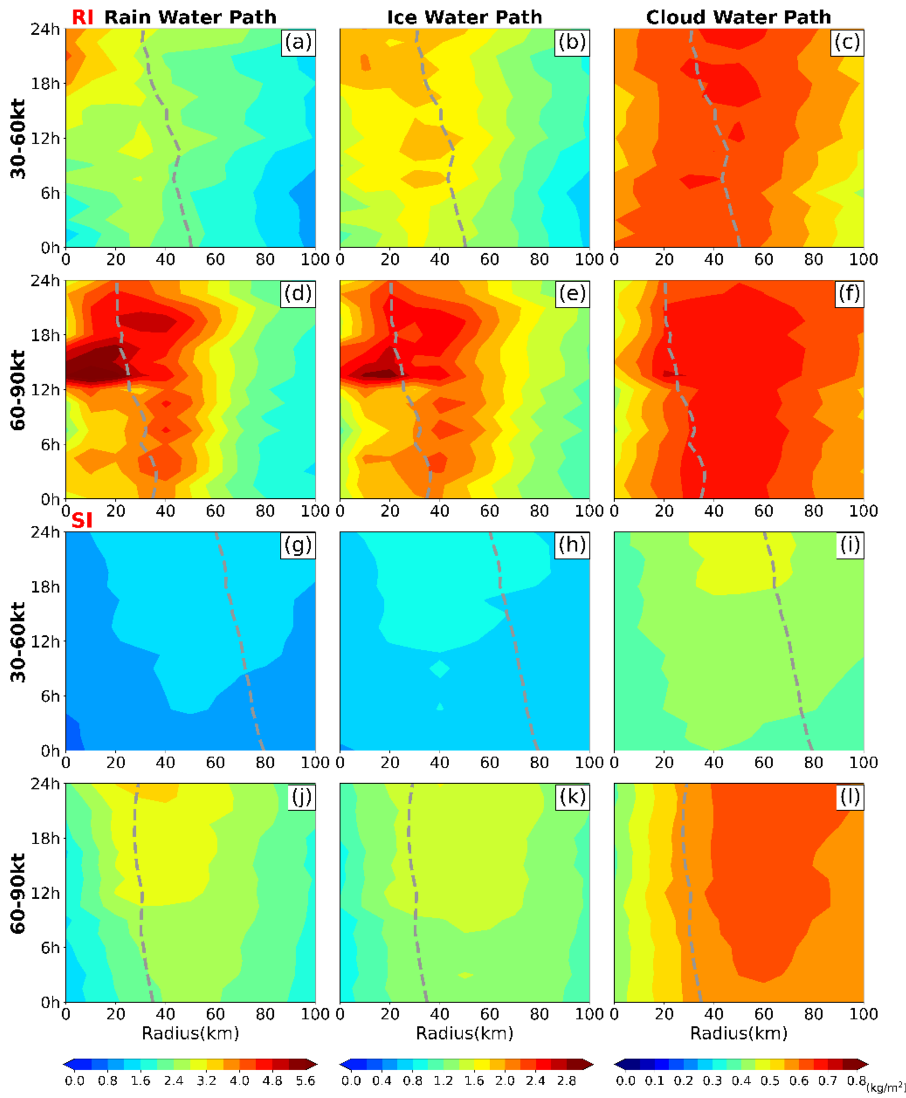

Fig. 2 Hovmöller diagrams of azimuthally averaged RWP (a,d,g,j), IWP(b,e,h,k), and CWP (c,f,i,l) (shaded, kg/m^2) in RI (a-f) and SI (g-l) for $TC_{30\text{-}60kt}$ and $TC_{60\text{-}90kt}$. The y-axis represents the time related to RI onset, and the x-axis represents the radius from the TC center. The gray dashed lines denote the RMW.

The maximum increasing rates of CWP in the inner-core regions of $TC_{60\text{-}90kt}$ and $TC_{30\text{-}60kt}$ during the RI are approximately the same. However, notably, the maximum rate of increase of CWP in the inner-core region of $TC_{30\text{-}60kt}$ during SI is comparable to that of $TC_{30\text{-}60kt}$ during RI, which is greater than that of $TC_{60\text{-}90kt}$ in SI (Fig. 1b-1c and Fig. 1f–1g). Owing to both the magnitude and location of the latent heat impact on TC intensification, the relationship between the RMW and hydrometeor distribution is examined. Fig. 2 shows that both the peak hydrometeor contents in $TC_{30\text{-}60kt}$ and $TC_{60\text{-}90kt}$ of RI are distributed near or within the RMW, while those of SI are distributed near or within the RMW of $TC_{30\text{-}60kt}$ and outside the RMW of $TC_{60\text{-}90kt}$. Although the peak hydrometeor contents of $TC_{30\text{-}60kt}$ in RI and SI are both within the RMW, the magnitude in RI is larger than that in SI (Fig. 2a-2c and Fig. 2g-2i), which is consistent with their intensification rates. A theoretical study by Schubert and Hack (1982) stated that the latent heat release from stronger TCs within the RMW results in higher intensification efficiencies. Fig. 2 is the observation appearance of the magnitude and location of latent heat release, RMW, TC intensity, and intensification rate. Owing to the offset of surface frictional dissipation, only when an appropriate latent heat increase at the right place is conducive to the maintenance and intensification of TC.

TC intensification is often related to the contraction of RMW (Shapiro & Willoughby, 1982; Schubert & Hack, 1982; Willoughby & Shoreibah, 1982; Quan et al., 2023). Fig. 2a-2f show that the RMW contraction is more evident in $TC_{30\text{-}60kt}$ than in $TC_{60\text{-}90kt}$ during RI. It is mainly due to the stronger curvature of RMW in strong TC than in weak TC. The contraction of RMW can be prohibited by increasing curvature of the RMW (Li et al., 2019). No significant difference in the RMW change is identified between the SI and RI (Fig. 2g-2l). This suggests that the contraction of RMW is a fundamental characteristic of TC intensification and the radius contraction rate is unrelated directly to the TC intensification rate.

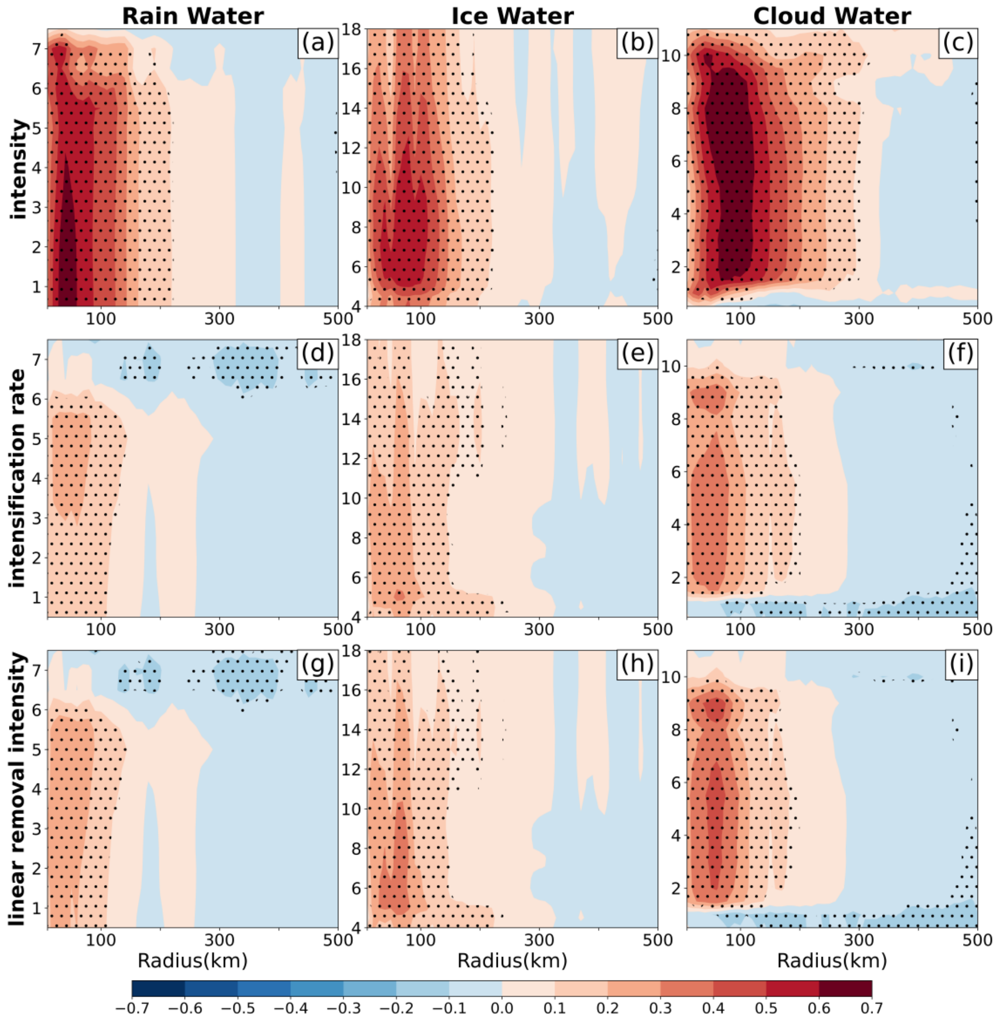

Fig. 3 Correlation coefficient radial profiles of azimuthal mean RWC, IWC, and CWC with TC intensity (a-c), intensification rate (d-f), and intensification rate after linearly removing the TC intensity effect (g-i). Dots denote the 99% confidence level of the correlation coefficient. The y-axis is the height (km), and the x-axis is the radius (km) from the TC center. Vertical areas with trifling hydrometeor content are omitted.

Wu et al. (2020) observed that tropical cyclones with an RI usually exhibit a larger IWC at the onset of intensification, emphasizing a strong correlation between the IWC near the storm center and the intensification rate. They have suggested that the IWC can serve as a predictor of the RI process. In this study, we calculated the correlation coefficients of all hydrometeor contents, including RWC, IWC, and CWC, with TC intensity and intensification rate for the intensifying cases (Fig. 3). The results show robust positive correlations between hydrometeors and TC intensity, primarily in the inner-core areas. CWC and RWC reveal the largest linear correlation coefficients in the lower and upper layers, respectively, and the former extended significantly to a radius of 300 km (Fig. 3a-3c). The IWC has the smallest linear correlation, although the radius of the significant correlation is approximately the same (200 km) as that of the RWC. The linear correlations between the hydrometeors and intensification rate (Figs. 3d-3f) are also significant, although with smaller coefficients. The radii of the maximum correlation coefficients between hydrometeors and intensity (Fig. 3a-3c) are shorter than those between hydrometeors and intensification rate (Figs. 3d-3f). This is the appearance of hydrometeor distribution on TC intensification, which is consistent with theoretical and simulation studies from various perspectives (Shapiro & Willoughby, 1982; Quan et al., 2023).

Theoretical and observational studies have demonstrated a close relationship between TC intensification rate and initial intensity (DeMaria, 2009; Xu & Wang, 2015). TC intensity exerts two effects on the intensification rate. The positive effect boosts the inertial stability in the eyewall region to enhance the heating efficiency, and the negative effect counteracts the effect of latent heating through frictional dissipation represented in the cube of the TC wind speed (Schubert and Hack., 1982; Wang et al., 2021). To examine the impact of TC intensity on the relationship between hydrometeors and the intensification rate, we remove the linear effect of TC intensity and recalculated the correlation. The correlation coefficients between the hydrometeors and intensification rates increase (Fig. 3g-3i). This indicates that TC intensity acts as a confounding factor for the relationship between the intensification rate and hydrometeor content, which should be considered in the prediction. As shown in Fig. 3i, the correlation coefficient associated with CWC exceeded 0.4, which is more significant than those for IWC and RWC. Fig. 3i has also shown that there are two maximum correlation coefficients in the middle and upper layers. This is similar to the modeling study of Li et al. (2019), in which two net heating peaks at 5 and 9 km are observed during the CB process in the RI, which are attributed to the associated peak value of the vertical velocity (Li et al., 2019; Qin et al., 2023).

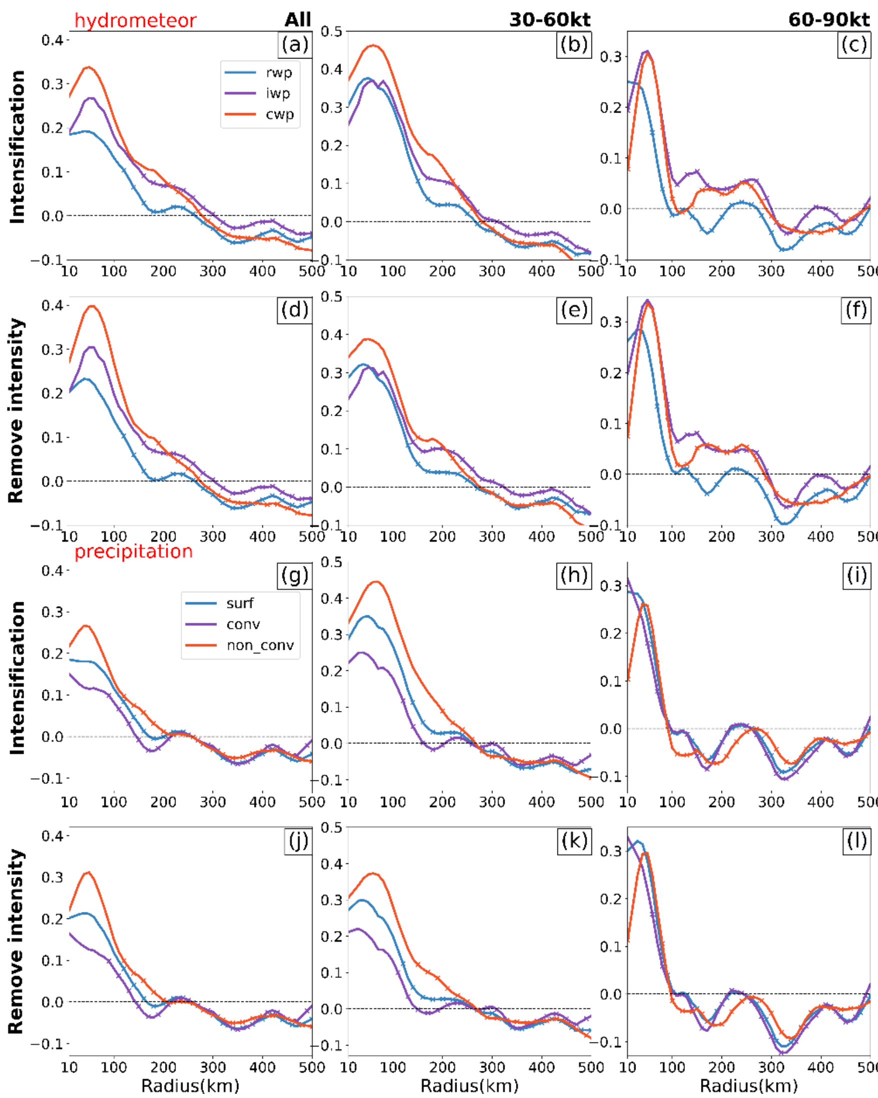

Fig. 4 Radial distribution of the correlation coefficients between the azimuthal-averaged column contents of hydrometeors and intensification rates (a-c) for all cases (a), $TC_{30\text{-}60kt}$ (b), and $TC_{60\text{-}90kt}$ (c); (d-f) are similar to (a-c), but after the removal of the TC intensity effect; (g-l) is similar to (a-f), but from the perspective of the precipitation rate. Lines marked with an "x" indicate not passing the 95% significance test.

How is surface precipitation related to the intensification rate compared with hydrometeors? Fig. 4 shows the correlation coefficients along the radius of precipitation and column hydrometeor content with the TC intensification rate based on the TC intensity. For all TCs, the correlation associated with non-convective precipitation has a larger coefficient than that with convective precipitation in the core region but smaller than that with CWP (Fig. 4a and 4g). In the $TC_{30\text{-}60kt}$ cases, the coefficient associated with CWP is the largest in the core region among RWP, IWP, and precipitation, although the difference between those associated with CWP and non-convective precipitation decreased compared to that of all cases (Fig. 4b and 4h). After linearly removing the TC intensity effect, the coefficients decrease (Fig. 4e and 4k), which is opposite to that for all TCs (Fig. 4d and 4j). However, the situation is different for the $TC_{60\text{-}90kt}$ cases, in which the CWP, IWP, and convective precipitation have similar correlation coefficients with the intensification rate of TC (Fig. 4c and 4i); after removal of the TC intensity effect, the coefficients increase, and those associated with CWP and IWP are slightly larger than others (Fig. 4f and 4l). The difference in performances between $TC_{30\text{-}60kt}$ and $TC_{60\text{-}90kt}$ is due to the relationship between the initial intensity and intensification rate of the TCs (Fig. S4), which has shown similar features in a study by Xu and Wang (2015). That is, a stronger initial intensity of the TC promotes a higher intensification rate in weak TCs, whereas for strong TC cases, a stronger initial intensity is associated with a lower intensification rate in the future. Keep in mind that the threshold for distinguishing between weak and strong TCs is defined based on the intensity at the peak of the curve representing the evolution of TC's intensification over the Western North Pacific (WNP). The threshold value varies with ocean region, with approximately 60 kts over WNP in this study and 80 kts in the North Atlantic [refer to Fig. 1a of Xu & Wang (2015)]. Fig. 4 reveals that the differences among previous studies may be partly affected by the TC intensity or the proportion of different TC intensities for a group of cases. Among all hydrometeors and precipitates, CWC might be a better precursor for rapid TC intensification, regardless of the TC intensity.

4 Conclusions

This study uses GPM satellite observations to examine the impact of TC intensity on hydrometeors and precipitation evolution characteristics during TC RI in the WNP. Generally, higher hydrometeor contents can be expected in RI cases than in SI cases, which increase with TC intensity. The hydrometeor content changes during the RI are larger than those during the SI. In the RI process, the hydrometeor contents of weak TC increase throughout the entire region. In contrast, those of strong TC significantly increase in the inner-core region in a short time while decreasing in the outer-core region, showing a feature of hydrometeor concentration towards the center. This implies that there are different increasing models for weak and strong TCs. Hydrometeors are mainly distributed within the RMW for weak TCs during intensification, whereas they are within the RMW during RI and outer RMW during SI for strong TCs. This shows that the relationship between the intensification rate of TC and hydrometeor content and location is intimately associated with TC intensity. Hydrometeors in the inner-core region are significantly correlated with the TC intensification rate; the peaks of the correlation coefficients are closer to the center than those correlations with TC intensity, indicating the characteristics of TC intensification. Among the hydrometeors, the correlation between the CWC in the inner-core region and the TC intensification rate is the most significant for all TCs. After linearly removing the intensity effect, the correlation coefficients increase for all TC groups and strong TCs, whereas it decreases for weak TCs, indicating that TC intensity interferes with the relationship between hydrometeors and intensification rate. From the precipitation perspective, non-convective precipitation is a better predictor than convective precipitation, although it is inferior to CWC. A comprehensive comparison suggests that the CWC in the core region of the TC is the best predictor of RI; however, the influence of TC intensity should also be considered. This study provides some observational features of hydrometeors in the RI with GPM. This supports previous studies on hydrometeors as predictors of TC intensification and further suggests that the CWC may serve as a better predictor of RI among all hydrometeors and precipitation, as well as the impact characteristics of TC intensity. Future research should explore the physical mechanisms of different hydrometeor evolutions in RI processes between weak and strong TC using high-resolution numerical simulations.

Acknowledgments

This study is supported by the National Natural Science Foundation of China (grant no.41930967).

Data Availability Statement

GPM satellite data are downloaded from the NASA Goddard Earth Sciences Data and Information Services Center (https://disc.gsfc.nasa.gov/datasets/GPM_2AGPROFGPMGMI_07/summary). The IBTrACS data are obtained from the National Centers for Environmental Information (https://www.ncei.noaa.gov/products/international-best-track-archive).

References

Adler, R. F., & Rodgers, E. B. (1977). Satellite-Observed Latent Heat Release in a Tropical Cyclone. *Monthly Weather Review*, *105*(8), 956–963. https://doi.org/10.1175/1520-0493(1977)105<0956:SOLHRI>2.0.CO;2

Cecil, D. J., & Zipser, E. J. (1999). Relationships between Tropical Cyclone Intensity and Satellite-Based Indicators of Inner Core Convection: 85-GHz Ice-Scattering Signature and Lightning. *Monthly Weather Review*, *127*(1), 103–123. https://doi.org/10.1175/1520-0493(1999)127<0103:RBTCIA>2.0.CO;2

Courtney, J. B., Langlade, S., Barlow, S., Birchard, T., et al., (2019). Operational perspectives on tropical cyclone intensity change Part II: forecasts by operational agencies, *Tropical Cyclone Research and Review*, *8*(4), 226-239, https://doi.org/10.1016/j.tcrr.2020.01.003

DeMaria, M. (2009). A Simplified Dynamical System for Tropical Cyclone Intensity Prediction. *Monthly Weather Review*, *137*(1), 68–82. https://doi.org/10.1175/2008MWR2513.1

DeMaria, M., Franklin, J. L., Onderlinde, M. J., & Kaplan, J. (2021). Operational Forecasting of Tropical Cyclone Rapid Intensification at the National Hurricane Center. *Atmosphere*, *12*(6), 683. https://doi.org/10.3390/atmos12060683

Elsberry, R. L., Lambert, T. D. B., & Boothe, M. A. (2007). Accuracy of Atlantic and Eastern North Pacific Tropical Cyclone Intensity Forecast Guidance. *Weather and Forecasting*, *22*(4), 747–762. https://doi.org/10.1175/WAF1015.1

Emanuel, K. (2018). 100 Years of Progress in Tropical Cyclone Research. *Meteorological Monographs*, *59*(1), 15.1-15.68. https://doi.org/10.1175/AMSMONOGRAPHS-D-18-0016.1

Fischer, M. S., Tang, B. H., Corbosiero, K. L., & Rozoff, C. M. (2018). Normalized Convective Characteristics of Tropical Cyclone Rapid Intensification Events in the North Atlantic and Eastern North Pacific. *Monthly Weather Review*, *146*(4), 1133–1155. https://doi.org/10.1175/MWR-D-17-0239.1

Harnos, D. S., & Nesbitt, S. W. (2016). Passive Microwave Quantification of Tropical Cyclone Inner-Core Cloud Populations Relative to Subsequent Intensity Change. *Monthly Weather Review*, *144*(11), 4461–4482. https://doi.org/10.1175/MWR-D-15-0090.1

Hou, A. Y., Kakar, R. K., Neeck, S., Azarbarzin, A. A., Kummerow, C. D., Kojima, M., Oki, R., Nakamura, K., & Iguchi, T. (2014). The Global Precipitation Measurement Mission. *Bulletin of the American Meteorological Society*, *95*(5), 701–722. https://doi.org/10.1175/BAMS-D-13-00164.1

Jiang, H., & Ramirez, E. M. (2013). Necessary Conditions for Tropical Cyclone Rapid Intensification as Derived from 11 Years of TRMM Data. *Journal of Climate*, *26*(17), 6459–6470. https://doi.org/10.1175/JCLI-D-12-00432.1

Kaplan, J., & DeMaria, M. (2003). Large-Scale Characteristics of Rapidly Intensifying Tropical Cyclones in the North Atlantic Basin. *Weather and Forecasting*, *18*(6), 1093–1108. https://doi.org/10.1175/1520-0434(2003)018<1093:LCORIT>2.0.CO;2

Kaplan, J., DeMaria, M., & Knaff, J. A. (2010). A Revised Tropical Cyclone Rapid Intensification Index for the Atlantic and Eastern North Pacific Basins. *Weather and Forecasting*, *25*(1), 220–241. https://doi.org/10.1175/2009WAF2222280.1

Kieper, M. E., & Jiang, H. (2012). Predicting tropical cyclone rapid intensification using the 37 GHz ring pattern identified from passive microwave measurements. *Geophysical Research Letters*, *39*(13). https://doi.org/10.1029/2012GL052115

Klotzbach, P. J., Wood, K. M., Schreck, C. J., Bowen, S. G., Patricola, C. M., & Bell, M. M. (2022). Trends in Global Tropical Cyclone Activity: 1990–2021. *Geophysical Research Letters*, *49*(6), e2021GL095774. https://doi.org/10.1029/2021GL095774

Knapp, K. R., Kruk, M. C., Levinson, D. H., Diamond, H. J., & Neumann, C. J. (2010). The International Best Track Archive for Climate Stewardship (IBTrACS): Unifying Tropical Cyclone Data. *Bulletin of the American Meteorological Society*, *91*(3), 363–376. https://doi.org/10.1175/2009BAMS2755.1

Li, M., Ping, F., Tang, X., & Yang, S. (2019). Effects of microphysical processes on the rapid intensification of Super-Typhoon Meranti. *Atmospheric Research*, *219*, 77–94. https://doi.org/10.1016/j.atmosres.2018.12.031

Li, Y., Tang, Y., Wang, S., Toumi, R., Song, X., & Wang, Q. (2023). Recent increases in tropical cyclone rapid intensification events in global offshore regions. *Nature Communications*, *14*(1), 5167. https://doi.org/10.1038/s41467-023-40605-2

Li, Y., Wang Y., and Lin Y., 2019: Revisiting the Dynamics of Eyewall Contraction of Tropical Cyclones. *J. Atmos. Sci.*, 76, 3229–3245. https://doi.org/10.1175/JAS-D-19-0076.1

Liu, C., Punay, J. P., Wu, C., Chung, K., & Aryastana, P. (2022). Characteristics of Deep Convective Clouds, Precipitation, and Cloud Properties of Rapidly Intensifying Tropical Cyclones in the Western North Pacific. *Journal of Geophysical Research: Atmospheres*, *127*(24), e2022JD037328. https://doi.org/10.1029/2022JD037328

Liu, K. S., & Chan, J. C. L. (2022). Growing Threat of Rapidly-Intensifying Tropical Cyclones in East Asia. *Advances in Atmospheric Sciences*, *39*(2), 222–234. https://doi.org/10.1007/s00376-021-1126-7

Lord, S. J., Willoughby, H. E., & Piotrowicz, J. M. (1984). Role of a Parameterized Ice-Phase Microphysics in an Axisymmetric, Nonhydrostatic Tropical Cyclone Model. *Journal of the Atmospheric Sciences*, *41*(19), 2836–2848. https://doi.org/10.1175/1520-0469(1984)041<2836:ROAPIP>2.0.CO;2

Miller, W., Chen, H., & Zhang, D.-L. (2015). On the Rapid Intensification of Hurricane Wilma (2005). Part III: Effects of Latent Heat of Fusion. *Journal of the Atmospheric Sciences*, *72*(10), 3829–3849. https://doi.org/10.1175/JAS-D-14-0386.1

Nolan, D. S., Moon, Y., & Stern, D. P. (2007). Tropical Cyclone Intensification from Asymmetric Convection: Energetics and Efficiency. *Journal of the Atmospheric Sciences*, *64*(10), 3377–3405. https://doi.org/10.1175/JAS3988.1

Nolan, D. S., Miyamoto, Y., Wu, S., & Soden, B. J. (2019). On the Correlation between Total Condensate and Moist Heating in Tropical Cyclones and Applications for Diagnosing Intensity. *Monthly Weather Review*, *147*(10), 3759–3784. https://doi.org/10.1175/MWR-D-19-0010.1

Pattnaik, S., & Krishnamurti, T. N. (2007). Impact of cloud microphysical processes on hurricane intensity, part 2: Sensitivity experiments. *Meteorology and Atmospheric Physics*, *97*(1–4), 127–147. https://doi.org/10.1007/s00703-006-0248-x

Qin, N., Wu, L., Liu, Q., & Zhou, X. (2023). Driving Forces of Extreme Updrafts Associated With Convective Bursts in the Eyewall of a Simulated Tropical Cyclone. *Journal of*

Geophysical Research: Atmospheres, *128*(6), e2022JD037061. https://doi.org/10.1029/2022JD037061

Quan, X., X. Li, and G. Zhai, 2023: Physical processes associated with movement of maximum winds of Typhoon Rammasun (2014). *Frontiers Earth Sci.*, *17*(2), 407-412. https://link.springer.com/article/10.1007/s11707-022-1003-4

Rodgers, E. B., Chang, S. W., & Pierce, H. F. (1994). A Satellite Observational and Numerical Study of Precipitation Characteristics in Western North Atlantic Tropical Cyclones. *Journal of Applied Meteorology and Climatology*, *33*(2), 129–139. https://doi.org/10.1175/1520-0450(1994)033<0129:ASOANS>2.0.CO;2

Rodgers, E. B., & Pierce, H. F. (1995). A Satellite Observational Study of Precipitation Characteristics in Western North Pacific Tropical Cyclones. *Journal of Applied Meteorology and Climatology*, *34*(12), 2587–2599. https://doi.org/10.1175/1520-0450(1995)034<2587:ASOSOP>2.0.CO;2

Rogers, R., Reasor, P., & Lorsolo, S. (2013). Airborne Doppler Observations of the Inner-Core Structural Differences between Intensifying and Steady-State Tropical Cyclones. *Monthly Weather Review*, *141*(9), 2970–2991. https://doi.org/10.1175/MWR-D-12-00357.1

Ruan, Z., & Wu, Q. (2018). Precipitation, Convective Clouds, and Their Connections With Tropical Cyclone Intensity and Intensity Change. *Geophysical Research Letters*, *45*(2), 1098–1105. https://doi.org/10.1002/2017GL076611

Randel, D. L., Kummerow, C. D., & Ringerud, S. (2020). The Goddard Profiling (GPROF) Precipitation Retrieval Algorithm. In V. Levizzani, C. Kidd, D. B. Kirschbaum, C. D. Kummerow, K. Nakamura, & F. J. Turk (Eds.), *Satellite Precipitation Measurement* (Vol. 1, pp. 141–152). Springer International Publishing. https://doi.org/10.1007/978-3-030-24568-9_8

Sawada, M., & Iwasaki, T. (2007). Impacts of Ice Phase Processes on Tropical Cyclone Development. *Journal of the Meteorological Society of Japan. Ser. II*, *85*(4), 479–494. https://doi.org/10.2151/jmsj.85.479

Schubert, W. H., & Hack, J. J. (1982). Inertial stability and tropical cyclone development. *Journal of the Atmospheric Sciences*, *39*(8), 1687-1697. https://doi.org/10.1175/1520-0469(1982)039<1687:ISATCD>2.0.CO;2

Song, J., Duan, Y., & Klotzbach, P. J. (2020). Increasing trend in rapid intensification magnitude of tropical cyclones over the western North Pacific. *Environmental Research Letters, 15*(8), 084043. https://doi.org/10.1088/1748-9326/ab9140

Shapiro, L. J., & Willoughby, H. E. (1982). The response of balanced hurricanes to local sources of heat and momentum. *Journal of the Atmospheric Sciences*, *39*(2), 378-394. https://doi.org/10.1175/1520-0469(1982)039<0378:TROBHT>2.0.CO;2

Su, H., Wu, L., Jiang, J. H., Pai, R., Liu, A., Zhai, A. J., Tavallali, P., & DeMaria, M. (2020). Applying Satellite Observations of Tropical Cyclone Internal Structures to Rapid Intensification Forecast With Machine Learning. *Geophysical Research Letters*, *47*(17), e2020GL089102. https://doi.org/10.1029/2020GL089102

Tang, X., Yang, S., Ping, F., Li, M., & Peng, J. (2019). Convection, latent heating and potential temperature budget in the rapidly intensifying Typhoon Mujigae (2015). *Atmospheric Science Letters*, *20*(9), e931. https://doi.org/10.1002/asl.931

Tao, C., & Jiang, H. (2015). Distributions of Shallow to Very Deep Precipitation–Convection in Rapidly Intensifying Tropical Cyclones. *Journal of Climate*, *28*(22), 8791–8824. https://doi.org/10.1175/JCLI-D-14-00448.1

Tao, C., Jiang, H., & Zawislak, J. (2017). The Relative Importance of Stratiform and Convective Rainfall in Rapidly Intensifying Tropical Cyclones. *Monthly Weather Review*, *145*(3), 795–809. https://doi.org/10.1175/MWR-D-16-0316.1

Vigh, J. L., & Schubert, W. H. (2009). Rapid Development of the Tropical Cyclone Warm Core. *Journal of the Atmospheric Sciences*, *66*(11), 3335–3350. https://doi.org/10.1175/2009JAS3092.1

Wang, Y. (2009). How Do Outer Spiral Rainbands Affect Tropical Cyclone Structure and Intensity? *Journal of the Atmospheric Sciences*, *66*(5), 1250–1273. https://doi.org/10.1175/2008JAS2737.1

Wang, H., & Wang, Y. (2014). A Numerical Study of Typhoon Megi (2010). Part I: Rapid Intensification. *Monthly Weather Review*, *142*(1), 29–48. https://doi.org/10.1175/MWR-D-13-00070.1

Wang, Y., Li, Y., Xu, J., Tan, Z.-M., & Lin, Y. (2021). The Intensity Dependence of Tropical Cyclone Intensification Rate in a Simplified Energetically Based Dynamical System Model. *Journal of the Atmospheric Sciences*, *78*(7), 2033–2045. https://doi.org/10.1175/JAS-D-20-0393.1

Weatherford C.L., W.M. Gray (1988). Typhoon structure as revealed by aircraft reconnaissance. Part I: Data analysis and climatology. *Monthly Weather Review*, 116(5), 1032-1043. https://doi.org/10.1175/1520-0493(1988)116<1032:TSARBA>2.0.CO;2

Weatherford C.L., W.M. Gray (1988). Typhoon structure as revealed by aircraft reconnaissance. Part II: Structural variability *Monthly Weather Review*, 116(5), 1044-1056. https://doi.org/10.1175/1520-0493(1988)116<1044:TSARBA>2.0.CO;2

Wu, S.-N., & Soden, B. J. (2017). Signatures of Tropical Cyclone Intensification in Satellite Measurements of Ice and Liquid Water Content. *Monthly Weather Review*, *145*(10), 4081–4091. https://doi.org/10.1175/MWR-D-17-0046.1

Wu, S. -N., Soden, B. J., & Alaka, G. J. (2020). Ice Water Content as a Precursor to Tropical Cyclone Rapid Intensification. *Geophysical Research Letters*, *47*(21), e2020GL089669. https://doi.org/10.1029/2020GL089669

Wu, Z., Zhang, Y., Zhang, L., & Zheng, H. (2023). Interaction of Cloud Dynamics and Microphysics During the Rapid Intensification of Super-Typhoon Nanmadol (2022) Based on Multi-Satellite Observations. *Geophysical Research Letters*, *50*(15), e2023GL104541. https://doi.org/10.1029/2023GL104541

Xu, J., & Wang, Y. (2015). A Statistical Analysis on the Dependence of Tropical Cyclone Intensification Rate on the Storm Intensity and Size in the North Atlantic. *Weather and Forecasting*, *30*(3), 692–701. https://doi.org/10.1175/WAF-D-14-00141.1

Zagrodnik, J. P., & Jiang, H. (2014). Rainfall, Convection, and Latent Heating Distributions in Rapidly Intensifying Tropical Cyclones. *Journal of the Atmospheric Sciences*, *71*(8), 2789–2809. https://doi.org/10.1175/JAS-D-13-0314.1

Zhang, D., Zhang, J., Yao, F., & Shi, L. (2019). Observed Characteristics Change of Tropical Cyclones During Rapid Intensification Over Western North Pacific Using CloudSat Data. *IEEE Journal of Selected Topics in Applied Earth Observations and Remote Sensing*, *12*(6), 1725–1733. https://doi.org/10.1109/JSTARS.2019.2917091

Zhao, D., Yu, Y., Yin, J., & Xu, H. (2020). Effects of Microphysical Latent Heating on the Rapid Intensification of Typhoon Hato (2017). *Journal of Meteorological Research*, *34*(2), 368–386. https://doi.org/10.1007/s13351-020-9076-z

Zhao, H., Duan, X., Raga, G. B., & Klotzbach, P. J. (2018). Changes in Characteristics of Rapidly Intensifying Western North Pacific Tropical Cyclones Related to Climate Regime Shifts. *Journal of Climate*, *31*(19), 8163–8179. https://doi.org/10.1175/JCLI-D-18-0029.1

Zhu, T., & Zhang, D.-L. (2006). Numerical Simulation of Hurricane Bonnie (1998). Part II: Sensitivity to Varying Cloud Microphysical Processes. *Journal of the Atmospheric Sciences*, *63*(1), 109–126. https://doi.org/10.1175/JAS3599.1